Theoretical and experimental study of pendular regime in unsaturated granular media

Gérard Gagneux, Olivier Millet, Boleslaw Mielniczuk, Moulay Saïd El Youssoufi

Theoretical and experimental study of pendular regime in unsaturated granular media

G. Gagneux[a], O. Millet[a]*, B. Mielniczuk[a,b] and M. S. El Youssoufi[b,c]

a LaSIE, UMR-CNRS 7356, University of La Rochelle, La Rochelle Cedex 1, France

b La boratoire de Mécanique et Génie Civil (LMGC), Université de Montpellier, CNRS, Montpellier, France

c Laboratoire de MicroMécanique et d'Intégrité des Structures MIST, IRSN, CNRS, Université de Montpellier, France

This article addresses the experimental study of capillary bridge properties with the use of analytical calculation of bridge profile, based on solution of Young–Laplace equation. Using the measurements of some parameters as the contact angle, half-filling angle and the neck radius of the capillary bridge between two spherical particles of radius r, the shape of the bridge is estimated using theoretical solutions of Young–Laplace equation. The corresponding analytical solution is superposed and compared with image data.

Keywords: capillary bridge; Young–Laplace equation; inverse problem; experimental measurement

1. Introduction

Capillary bridge, liquid link between solid particles, gives origin of several phenomena observed in unsaturated granular materials, connected always with interparticle capillary forces. These forces contribute to the formation, deformation and flow of granular materials (soils, powders, photonic crystal production, etc.). They impart an apparent macroscopic strength (sand castle effect) to the moist granular materials, even in the absence of the intrinsic cohesion or confining stress (see e.g. Peron, Delenne, Laloui and El Youssoufi 2009, Princen 1968, Gili and Alonso 2002). The most elementary liquid bridge is a pendular bridge, between two solid grains. The profile and evolution of pendular capillary bridge has been analysed for over 100 years from theoretical and experimental point of view (see e.g. Young 1805, Plateau, 1864, Mason and Clark, 1965, Haines, 1925, Megias-Alguacil and Gauckler, 2009, Lian, Thornton and Adams 1993, Willett, Adams, Johnson and Seville, 2000, Rabinovich, Esayanur and Moudgil, 2005, Soulie, Cherblanc, El Youssoufi and Saix, 2006, Gras, Delenne and El Youssoufi, 2013).

This article addresses the experimental study of the capillary bridge properties with use of the analytical calculation of bridge profile, based on solution of Young–Laplace equation (Gagneux and Millet, 2014). In this method, the parameters of pendular bridge and the shape of the meridian may be estimated using theoretical solutions of Young–Laplace equation, based on an inverse problem as the capillary pressure[1] is unknown (Gagneux & Millet 2014). However, this pressure may be recovered with experimental

measurements of three geometrical parameters: gorge radius y^*, contact angle θ, half-filling angle δ. This will be done using experimental set-up similar to one described in Mielniczuk, Hueckel, El Youssoufi (2013, 2014, 2015). In this paper, we focus on the evolution of capillary bridge profile and associated mean curvature. Calculations of capillary force and Laplace pressure will constitute the subject of a next paper.

For a fixed volume, a capillary bridge between two spheres is created for a separation distance D close to zero. Then, the separation distance is increased up to the rupture of the bridge. For several distances D, a photo of the capillary bridge is recorded and the geometric parameters (y^*, δ, θ) are measured from image processing. Then shape of the capillary bridge, and its exact analytical parameterisation, are deduced, according to the criterion given in Gagneux and Millet 2014 and recalled in Section 2. The shapes obtained correspond, first to a portion of nodoid (from the creation of the capillary bridge to some distance D). Then, when the separation distance increases, the shape of the capillary bridge skips to a portion of unduloid before rupture. The catenoid shape which constitutes a limit case of the nodoid–unduloid transition, has not been observed in the experiments performed in this study (it does not correspond to a stable configuration). Concave shapes (and cylinder shape) also exist but do not correspond neither to stable case. Note that for microscopic bubbles, the use of the theory of second gradient fluids is necessary to take into account microscopic effects, not concerned in this study (dell'Isola, Gouin and Seppecher, 1995).

2. Theoretical framework

We recall briefly the main results on capillary bridge properties obtained from analytical calculations of Young–Laplace equation. The reader may find more details in Gagneux and Millet (2014). Seven shapes of the meridian, with constant mean curvature, are possible according to the filling and contact angles δ and θ, and to the radius of the capillary bridge neck y^* (Delaunay, 1841; Gagneux & Millet, 2014). The capillary pressure at the right-hand side of the Young–Laplace equation is reconstituted from the given data (y^*, δ, θ) according to the following procedure.

Let us start again from the Young–Laplace equation which can be written as follows:

$$\frac{y''}{(1+y'^2)^{3/2}} - \frac{1}{y\sqrt{1+y'^2}} = -\frac{\Delta p}{\gamma} =: H \tag{1}$$

where Δp is the pressure difference between inside and outside of the capillary bridge, γ is the surface tension and $x \mapsto y(x)$ specifies (the shape of) the upper meridian of the capillary bridge. The integration of Young–Laplace equation leads to the non-linear first-order differential equation when[2] $H \neq 0$ (Gagneux & Millet, 2014)

$$1 + y'^2 = \frac{4y^2}{H^2\left(y^2 - \frac{2\lambda}{H}\right)^2} \tag{2a}$$

where λ defined by

$$\lambda = \frac{y}{\sqrt{1+y'^2}} + \frac{Hy^2}{2} \tag{2b}$$

is remarkably constant on a given Delaunay profile (Delaunay, 1841; Gagneux & Millet, 2014). It constitutes a first integral of the Young–Laplace equation (in fact, an energy

conservation law). The associated capillary force may be calculated at the neck radius y^* as follows:

$$F_{cap} = \pi\gamma H y^{*2} + 2\pi\gamma y^* = 2\pi\gamma\lambda \tag{3}$$

According to the signs of H and λ, Equation (2) corresponds to one that governs the Delaunay roulettes (Delaunay, 1841)

$$1 + y'^2 = \frac{4a^2y^2}{(y^2 + \epsilon b^2)^2} \tag{4}$$

The case $\epsilon = 1$ corresponds to a portion of unduloid, whereas the case $\epsilon = -1$ corresponds to a portion of nodoid.

In this article, only pendular bridges between two spherical grains of radius r are examined. We limit our study to concave capillary bridge with convex upper meridian satisfying $y^* \leq r \sin\delta$ (Figure 1).

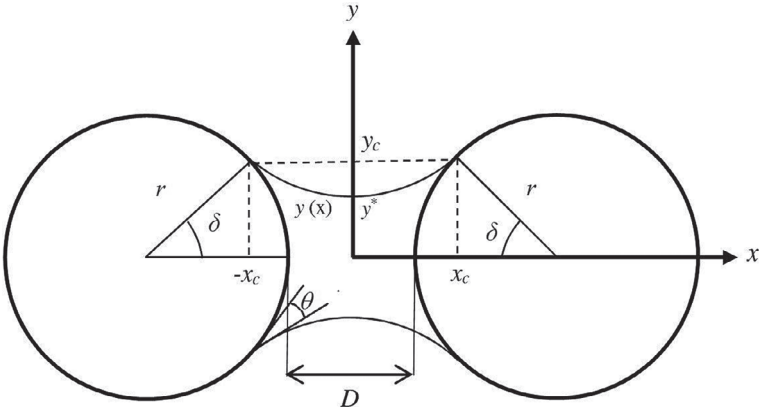

Figure 1. Convex profile of a capillary bridge.

Moreover, we only focus on nodoid and unduloid capillary bridges which correspond to the main stable cases observed experimentally. The criterion of determination of the shape is recalled in the following results.

Result 1. If the observed data (y^*, δ, θ) are such that

$$r\sin\delta\sin(\delta + \theta) < y^* < r\sin\delta \tag{5}$$

with $H > 0$ and $\lambda > 0$, then the meridian of the capillary bridge is a portion of nodoid whose parameterisation is given by

$$x(t) = \frac{b^2}{a}\int_0^t \frac{\cos u\,\mathrm{d}u}{(e + \cos u)\sqrt{e^2 - \cos^2 u}} \tag{6a}$$

$$y(t) = b\sqrt{\frac{e - \cos t}{e + \cos t}}, \quad t \in [-\tau,\ \tau] \tag{6b}$$

where

$$e = \frac{\sqrt{a^2 + b^2}}{a} \ , \tau = \arccos\left(e \frac{b^2 - r^2 \sin^2 \delta}{b^2 + r^2 \sin^2 \delta} \right) \tag{6c}$$

is the unique solution in $(0,\ \pi/2)$ of equation $y(\tau) = r \sin \delta$. The associated geometrical parameters are given by

$$a = \frac{1}{2} \frac{r^2 \sin^2 \delta - y^{*2}}{y^* - r \sin \delta \sin(\delta + \theta)} \tag{7a}$$

$$b^2 = y^* r \sin \delta \frac{r \sin \delta - y^* \sin(\delta + \theta)}{y^* - r \sin \delta \sin(\delta + \theta)} \tag{7b}$$

The capillary pressure Δp and the mean curvature H may be calculated as follows:

$$\Delta p = -2\gamma \ \frac{y^* - r \sin \delta \ \sin(\delta + \theta)}{r^2 \sin^2 \delta - y^{*2}}, \quad H = -\frac{\Delta p}{\gamma} = \frac{1}{a} \tag{8}$$

Result 2. If the observed data (y^*, δ, θ) are such that

$$0 < y^* < r \sin \delta \sin(\delta + \theta) \tag{9}$$

with $H < 0$ and $\lambda > 0$, then the meridian of the capillary bridge is a portion of unduloid whose parameterisation is given by:

$$x(t) = \frac{b^2}{a} \int_0^t \frac{\mathrm{du}}{(1 + e \cos u)\sqrt{1 - e^2 \cos^2 u}} \tag{10a}$$

$$y(t) = b \sqrt{\frac{1 - e \cos t}{1 + e \cos t}}, \quad t \in [-\tau',\ \tau'] \tag{10b}$$

where

$$e = \frac{\sqrt{a^2 + b^2}}{a}, \quad \tau' = \arccos\left(\frac{1}{e} \frac{b^2 - r^2 \sin^2 \delta}{b^2 + r^2 \sin^2 \delta} \right) \tag{10c}$$

is a unique solution in $(0,\ \pi/2)$ of equation $y(\tau') = r \sin \delta$. The geometrical parameters are given by:

$$a = \frac{1}{2} \frac{r^2 \sin^2 \delta - y^{*2}}{r \sin \delta \sin(\delta + \theta) - y^*} \tag{11a}$$

$$b^2 = y^* r \sin \delta \frac{r \sin \delta - y^* \sin(\delta + \theta)}{r \sin \delta \sin(\delta + \theta) - y^*} \tag{11b}$$

The capillary pressure Δp and the mean curvature H may be calculated as follows:

$$\Delta p = \frac{\gamma}{a}, \quad H = -\frac{1}{a}. \tag{12}$$

3. Experiments

The experiments are performed on a pair of monodispersed borosilicate glass spherical grains, with grade 25% (precision of diameter $\pm 2.5\,\mu m$, precision of sphericity $\pm 0.625\,\mu m$), with diameter of 8 mm. Experiments are difficult to carry out for smaller diameters of grains (difficulties for positioning the spheres, of for injecting very small water volume). The experiment addresses the series of tests with fixed liquid volume and varying (increasing) interparticle distances. The total time of our experiment is no more than about 3 min. During this time, the decrease of the volume caused by evaporation is only a few per cent and it can be neglected in our calculations.

During experiments, both spheres are fixed vertically one over another, with use of two aluminium supports. The separation distance D between the spheres is controlled using a micrometre stage, while its vertical alignment is adjusted using optical system and X–Y micrometre stage. Before each experiment, the surface of the spheres is cleaned using 99% ethanol and it is left for several minutes to totally evaporate. The initial separation distance between the particles is set to zero (spheres in contact). The water drop of the given volume (from 1 to 10 µl) is then introduced between them using laboratory micro-syringe (precision of 0.1 µl) to form a symmetric liquid bridge. Then distance D is increased by steps of 0.1 mm, until the bridge is broken down. At each distance, after short time needed for bridge stabilisation (about 5 s) the photo of the created capillary bridge is taken.

During tests a photo camera Nikon D5300 with macro-lens and the resolution of 24 Mpixels is used. To obtain the best possible contrast between bridge profile and background, LED-type backlight is applied (LED matrix). The images are recorded using Nikon Camera Control Pro software which allows to visualise directly the image, to adjust camera parameters and to take photos without physical contact with photo camera. The original photo is saved in JPG format of a very high quality with resolution of 4000×6000 pixels and then adjusted and treated as described below. The scheme of experimental configuration is presented in Figure 2. To calculate the physical variables, all geometrical parameters are converted from pixels to millimetres, with calibration of photo camera using micrometre stage (calibration slide), with the resolution of 0.01 mm.

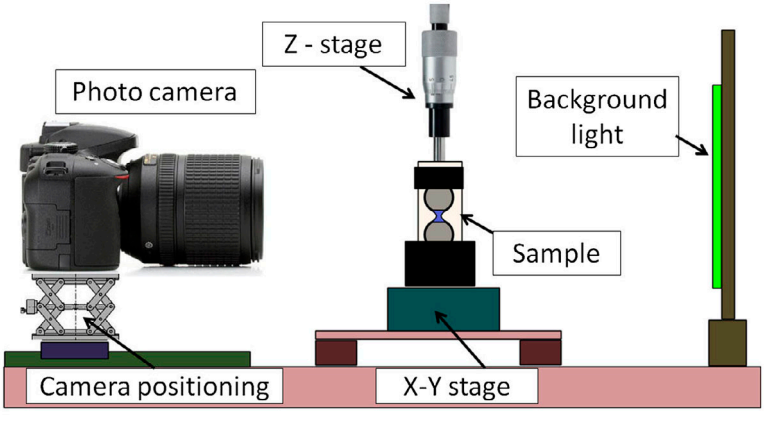

Figure 2. Configuration of experimental apparatus.

4. Image analysis and geometrical characteristics of the capillary bridge

In this section, the image treatment procedure is described. For each tested volume of the bridge, the sequence from 20 to 50 photos is obtained, depending on the volume and of the rupture distance (one photo for each separation distance). Each image is than adjusted with the help of image treatment tool *imageJ*. The part of the photo is cropped (Figure 3), image is binarised using threshold option and the edges are detected. The final image is represented as a table **A** of 1 for contour and 0 otherwise. Such image is used with Matlab code.

Basing on prepared images, we define a domain Ω within which the capillary bridge is situated, as shown in Figure 4(a)), limited by x_{up} and x_{low} coordinates (Figure 3(b)). Arrays with coordinates of sphere profiles are constructed for upper and lower spheres (above and below capillary bridge domain). Then centers $c_1 = (x_{c_1}, y_{c_1})$, $c_2 = (x_{c_2}, y_{c_2})$ and radius r (mean value of both spheres radii R_{c_1}, R_{c_2}) are determined (Figure 4(a)), using the code proposed by Taubin (1991). The mean radius r is used in further calculations. The coordinates of liquid bridge correspond to the first and the last non-zero element of $\{\mathbf{A}(i,j)|\{i,j\} \in \Omega\}$ (Figure 4(a)), with exclusion of the points which are on the spheres surface (within some numerical error ε):

$$(x - x_{c_1})^2 + (y - y_{c_1})^2 > (r \pm \varepsilon)^2 \;\&\; (x - x_{c_2})^2 + (y - y_{c_2})^2 > (r \pm \varepsilon)^2 \tag{13}$$

The coordinates of left and right sides of the capillary bridge profile,[3] denoted by $Y_L(x)$ and $Y_R(x)$, respectively, are determined from image processing. Then the intersection with the sphere contour enables to determine the corresponding triple points p_1 to p_4 (Figure 4(b)), satisfing also Equation (13). The neck radius y^* is determined as a half of minimal distance between the left and right profile

$$y^* = \frac{1}{2} \min_{x \in [-x_x, x_c]} \{Y_R(x) - Y_L(x)\} \tag{14}$$

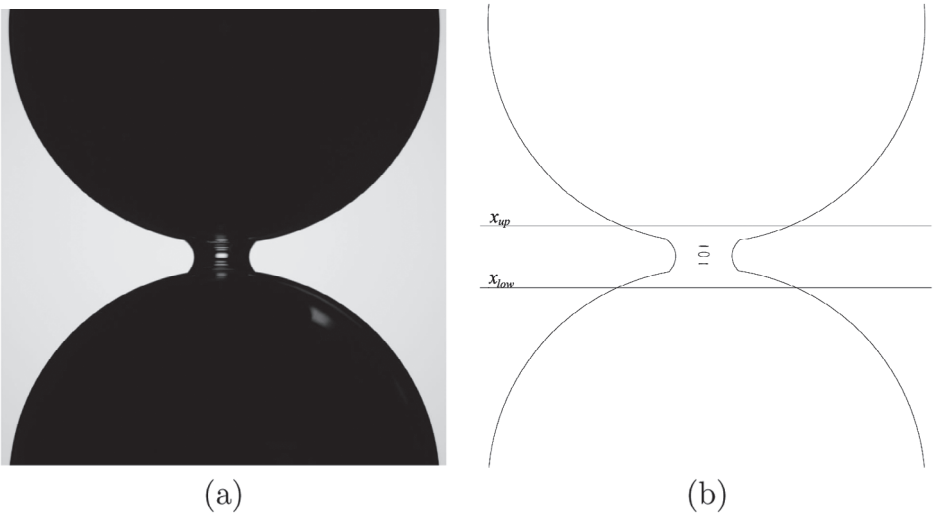

Figure 3. Example of the original photo after adjusting size (a) and final image (binarised) used for calculation of the bridge properties (b).

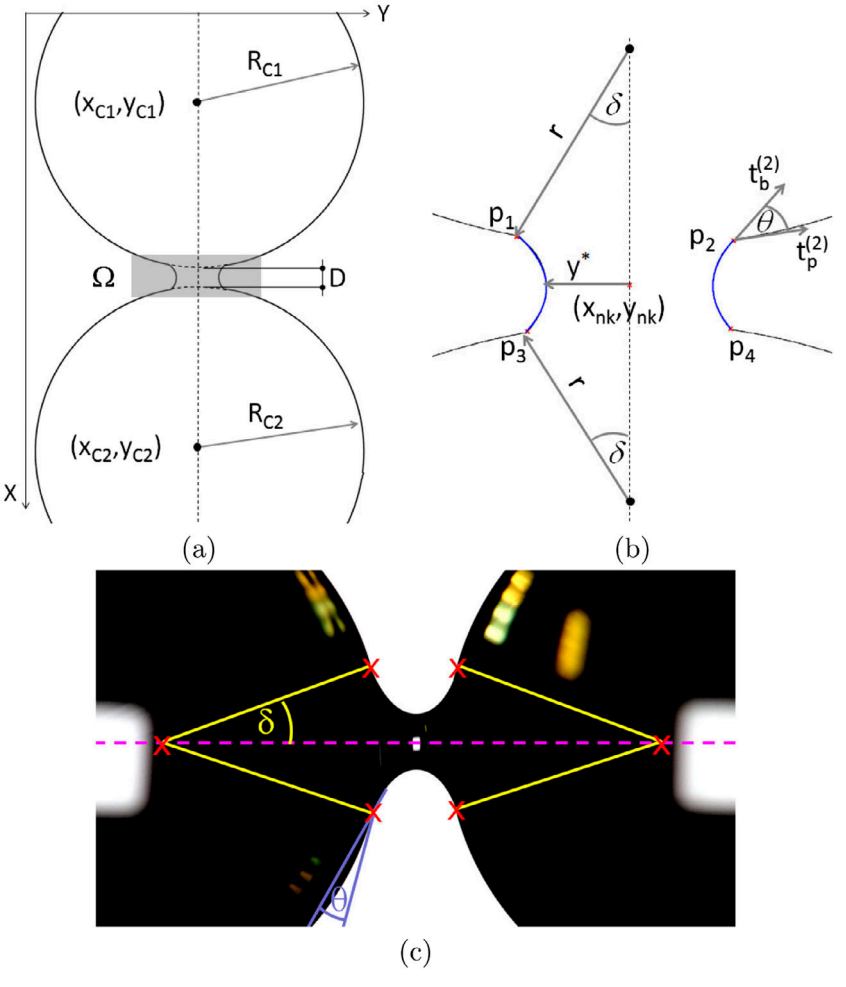

Figure 4. The process of the image analysis for the detection of the capillary bridge characteristics: detection of the particles positions (a) and of the bridge surface and the neck radius y^* (b). Overall view of contact angle θ and half-filling angle δ (c).

corresponding to the position x_{nk} on $x-$axis. Hence, the half-filling angles[4] δ_j are found for each triple point p_j by

$$\delta_j = \begin{cases} \pm \arctan\left(\frac{y_{p_j}-y_{c_1}}{x_{p_j}-x_{c_1}}\right), & j = 1,2 \\ \pm \arctan\left(\frac{y_{p_j}-y_{c_2}}{x_{p_j}-x_{c_2}}\right), & j = 3,4 \end{cases} \tag{15}$$

The resulting half-filling angle δ is found as an average over all δ_j (Figure 4(c)).

The next step is finding the contact angle θ (Figure 4(b) and (c)). To do this, we use the tangent vector to the sphere $\mathbf{t}_p^{(j)}$ and to the capillary bridge profiles $\mathbf{t}_b^{(j)}$ at the triple point j, pointing outside the bridge (Figure 4(b)). Then, the contact angles for each triple point are found as follows:

$$\theta_j = \arccos\left(\mathbf{t}_b^{(j)} \cdot \mathbf{t}_p^{(j)}\right), \quad j = 1, \ldots, 4 \tag{16}$$

The tangents to the sphere profiles $\mathbf{t}_p$ are found using the property

$$\mathbf{t}_p^{(j)} = \pm\left(\cos\delta_j, \pm\sin\delta_j\right) \tag{17}$$

In order to determine the tangent $\mathbf{t}_b^{(j)}$ to the capillary bridge profile, the latter is approximated by a sixth-degree polynomial (or by a linear approximation for several end points)[5]. The sign is chosen in order to obtain the $\mathbf{t}_p^{(j)}$ and $\mathbf{t}_b^{(j)}$ pointing outside the bridge, as shown in Figure 4(b)). The resulting contact angle θ is taken as an average over all θ_j, $j \in \{1, 2, 3, 4\}$. With the determined geometrical parameters ($y^*, \delta,\ \theta$), the criterion for determining the shape of capillary bridge (given in Results 1 and 2) is checked and the corresponding parameters a and b^2 are calculated. Then, the resulting parameterised curves (portion of nodoid or of unduloid) are plotted on the same image of the capillary bridge profile obtained experimentally and compared in Figures 6–9.

5. Experimental results

Using the procedure described in Section 4, the experimental data are analysed for examined configurations. Measured geometrical parameters are used to determine the type of fitting curve (nodoid or unduloid), to reconstruct and to trace the bridge profile using equations presented in Section 2. The evolution of the capillary bridge profile and of the associated mean curvature H are plotted in the function of interparticle distance D, for two examined diameters. The results are presented in Figures 5–9.

5.1. Mean curvature

The mean curvature H of the profile, presented in Figure 5, is calculated with use of equations (8) and (12).The sign of H determines the type of Delaunay roulette which

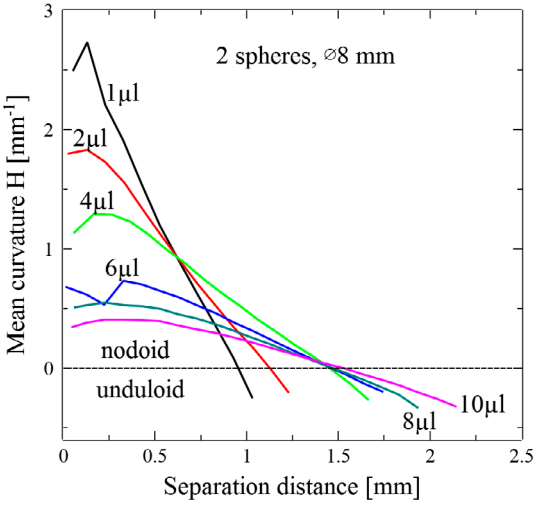

Figure 5. Mean curvature H of capillary bridge in function of interparticle distance D for the sphere of 8 mm diameter. $H > 0$ corresponds to the nodoid case and H to the unduloid one.

defines the meridian of the capillary bridge: a portion of nodoid for positive values of H or a portion of unduloid for negative values of H. For a fixed volume, the mean curvature changes with change of separation distance. For a given volume V, H is initially positive and decreases almost linearly in function of separation distance D. For small volumes, the slope of the curve $H(D)$ is higher than for larger volumes. In all the cases

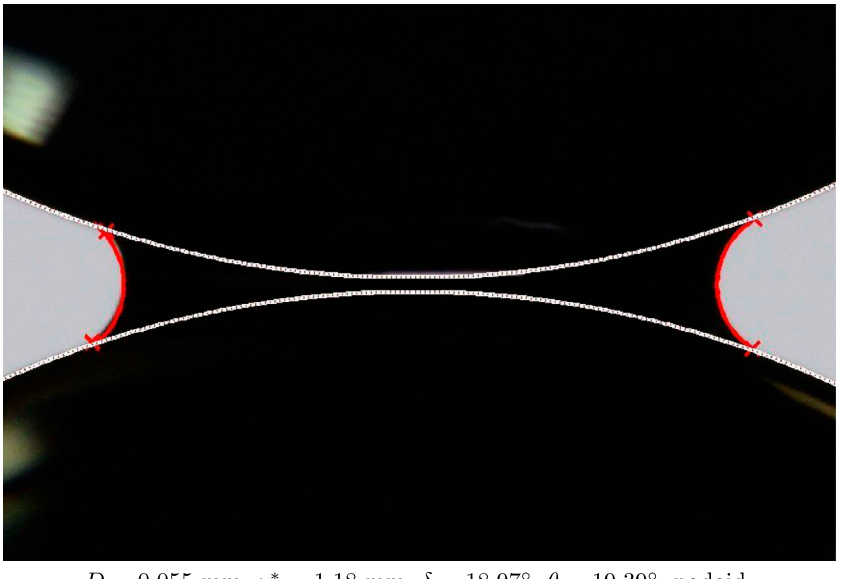

$D = 0.055$ mm, $y^* = 1.18$ mm, $\delta = 18.97°$, $\theta = 19.39°$, nodoid

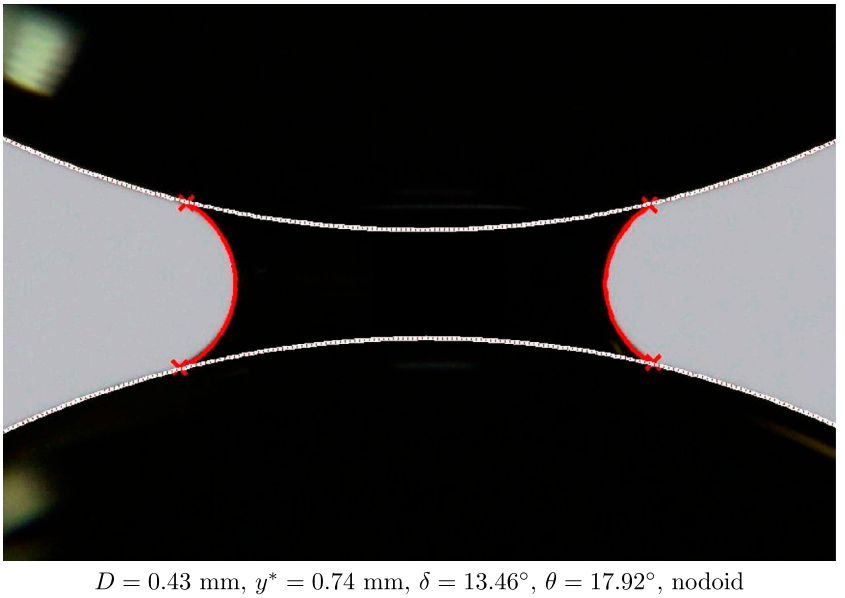

$D = 0.43$ mm, $y^* = 0.74$ mm, $\delta = 13.46°$, $\theta = 17.92°$, nodoid

Figure 6. Resulting bridge profiles superposed on the original images for glass spheres of 8 mm. The data are for fixed volume $V = 1\mu l$ and various distance D between particles (red: nodoid shape calculated from theory).

analysed, the mean curvature H passes through zero and becomes negative before the rupture of the bridge. The negative values of H (corresponding to a portion of unduloid) are attempted for about 80% of the final separation D for 8 mm beads.

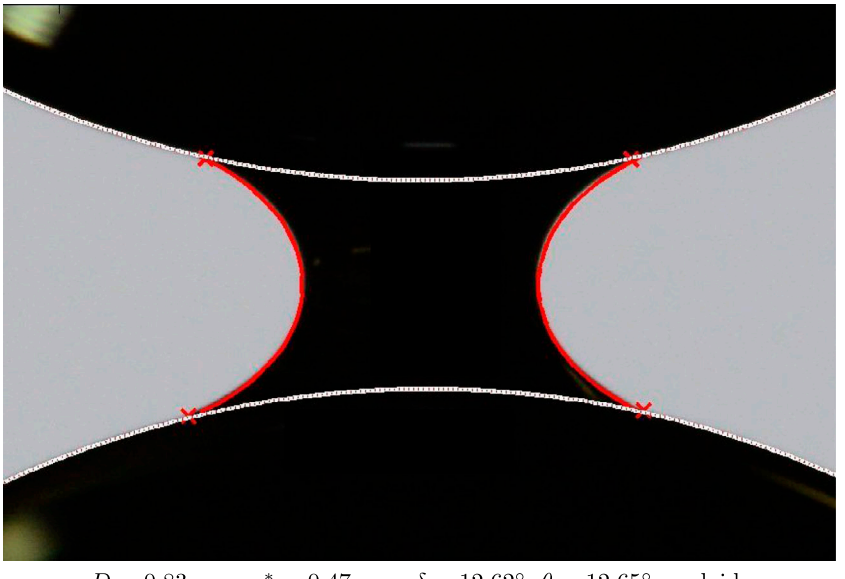

$D = 0.83$ mm, $y^* = 0.47$ mm, $\delta = 12.62°$, $\theta = 12.65°$, nodoid

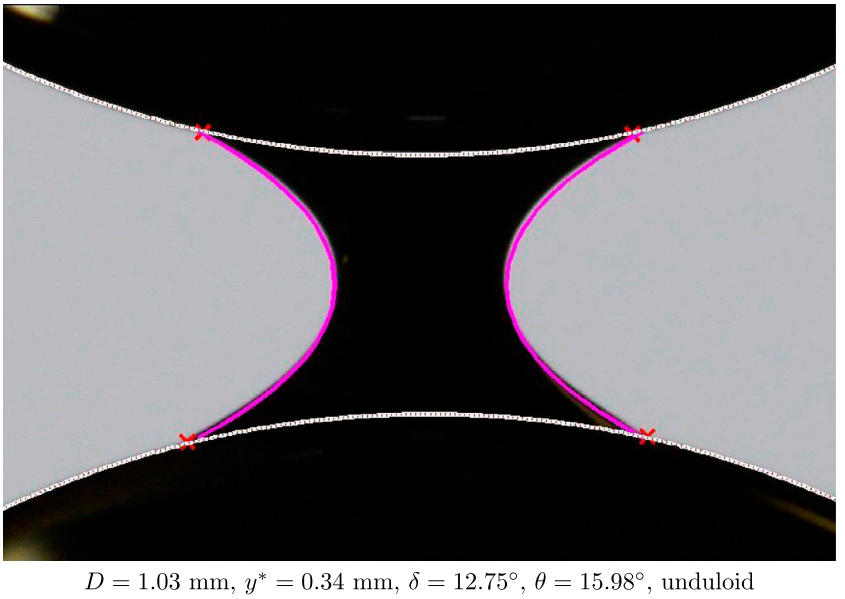

$D = 1.03$ mm, $y^* = 0.34$ mm, $\delta = 12.75°$, $\theta = 15.98°$, unduloid

Figure 7. Resulting bridge profiles superposed on the original images for glass spheres of 8 mm. The data are for fixed volume $V = 1\mu l$ and various distance D between particles (red: nodoid shape, blue: unduloid shape, calculated from theory).

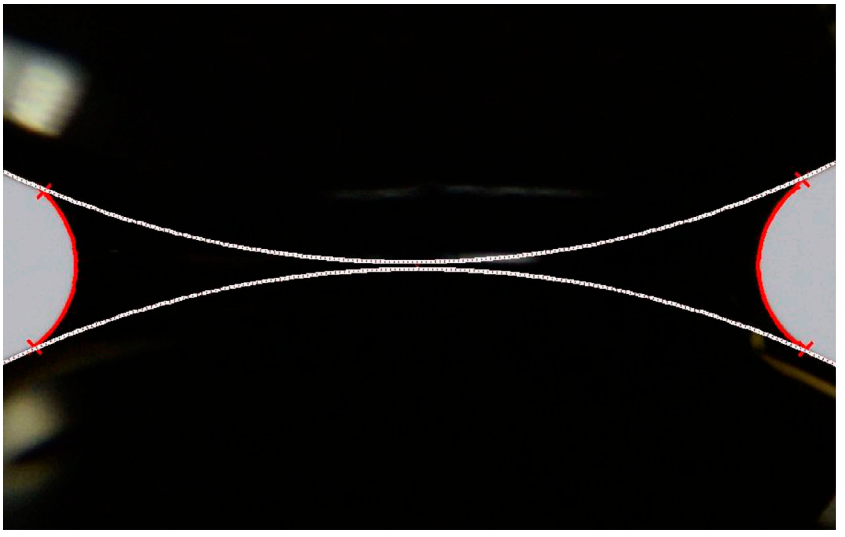

$D = 0.028$ mm, $y^* = 1.42$ mm, $\delta = 23.44°$, $\theta = 13.86°$, nodoid

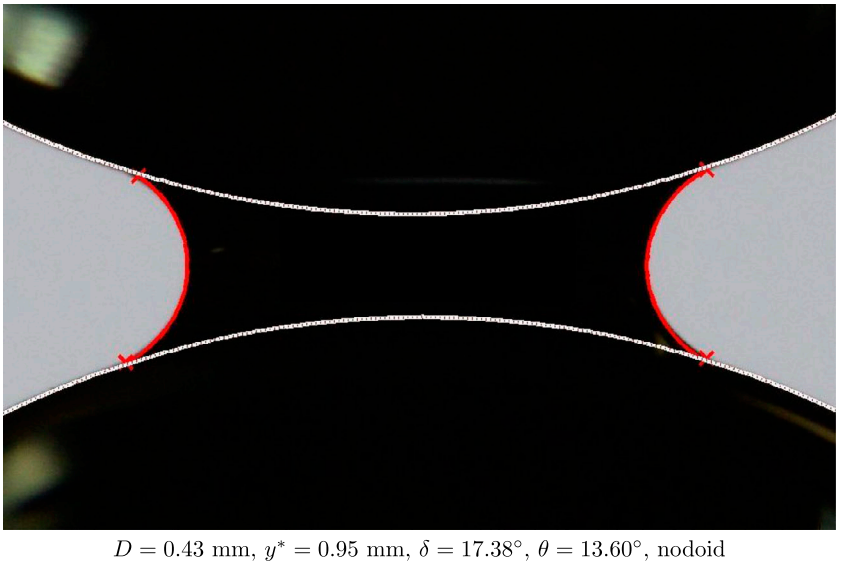

$D = 0.43$ mm, $y^* = 0.95$ mm, $\delta = 17.38°$, $\theta = 13.60°$, nodoid

Figure 8. Resulting bridge profiles superposed on the original images for glass spheres of 8 mm. The data are for fixed volume $V = 2\mu l$ and various distance D between particles (red: nodoid shape calculated from theory).

5.2. Capillary bridge profiles

To visualise the profiles of capillary bridges, the type of obtained profile is classified using the criterion (5) or (9). Then, the Delaunay roulettes parameters a and b^2 are found according to (7) for nodoids and (11) for unduloids. Sequence of separations with marked contact points, as well as bridge meridians calculated from theory, are presented in Figures 6–9.

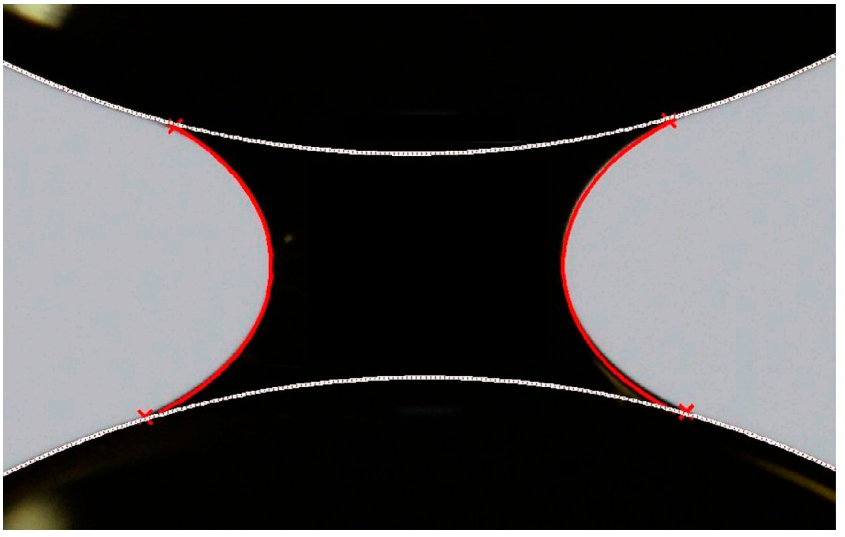

$D = 0.93$ mm, $y^* = 0.61$ mm, $\delta = 15.61°$, $\theta = 10.54°$, nodoid

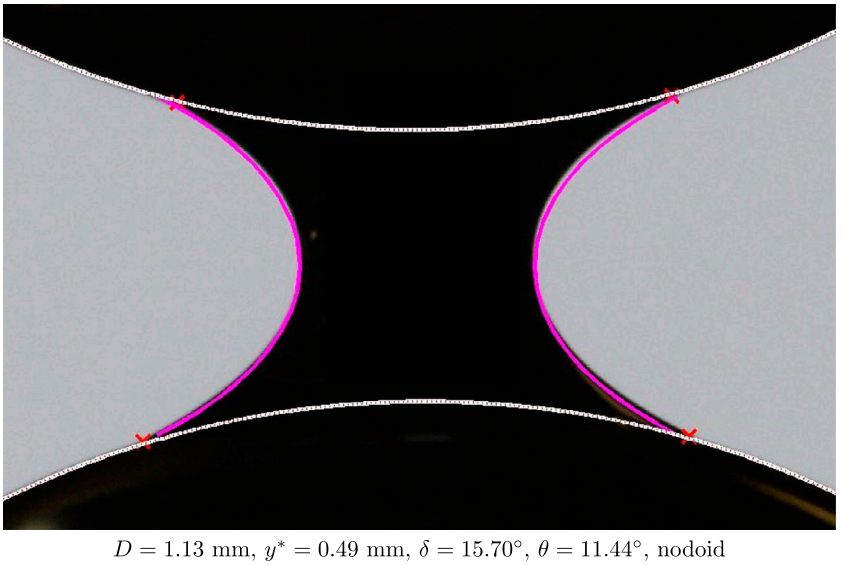

$D = 1.13$ mm, $y^* = 0.49$ mm, $\delta = 15.70°$, $\theta = 11.44°$, nodoid

Figure 9. Resulting bridge profiles superposed on the original images for glass spheres of 8 mm. The data are for fixed volume $V = 2\mu l$ and various distance D between particles (red: nodoid shape, blue: unduloid shape, calculated from theory).

In order to estimate the accuracy of method of analyse proposed, the maximal relative error between the observed bridge profile and the corresponding exact parameterisation given by the Delaunay roulettes, defined by (6) or (10), is analysed. For the nodoidal profiles, the error does not exceed 6.3%.

For higher separation distance, higher water volumes or higher diameter of spheres, the capillary bridges obtained experimentally are distorted, with more liquid placed in the bottom part of the bridge.[6] This loose of symmetry is due to the gravity effect on

the liquid, the Bond number (Adams, Johnson, Seville and Willett, 2002) being larger than in the examples addressed in this study.

6. Conclusions

The results from theoretical modelling match very accurately experimental results for small liquid volumes and small separations between particles. For larger ones, the capillary bridge loses its symmetry due the effects of gravity. In order to remove the distortion effect due to gravity, some experiments in microgravity in a parabolic flight[7] have been performed. The results obtained will be presented in the next work.

Acknowledgements

The authors acknowledge Iryna Malinouskaya for her help to develop the Matlab programm of image processing. The authors would like to express their sincere thanks to the French Research Network MeGe (Multiscale and multi-physics couplings in geo-environmental mechanics GDR CNRS 3176/2340, 2008-2015) for having supported this work.

Disclosure statement

No potential conflict of interest was reported by the authors.

Notes

1. At the right-hand side of Young–Laplace Equation (1).
2. Catenoid and catenary cases are not included in this study.
3. Or upper and lower sides if referring to Figure 1.
4. All chosen positive.
5. 1/40 of the total point number.
6. These cases are not presented here.
7. On an Airbus ZeroG of Novespace society and CNES.

References

Adams, M. J., Johnson, S. A., Seville, J. P. K., & Willett, C. (2002). Mapping the influence of gravity on pendular liquid bridges between rigid spheres. *Langmuir, 18*, 6180–6184.

Delaunay, C. H. (1841). Sur la surface de révolution dont la courbure moyenne est constante. *Journal de mathématiques pures et appliquées, 6*, 309–314.

dell'Isola, F., Gouin, H., & Seppecher, P. (1995). Radius and surface tension of microscopic bubbles by second gradient theory. *Comptes Rendus de l'Academie de Sciences – Serie IIb Mecanique, Physique, Chimie, Astronomie, 320*, 211–216.

Gagneux, G., & Millet, O. (2014). Analytic calculation of capillary bridge properties deduced as an inverse problem from experimental data. *Transport in Porous Media, 105*, 117–139. doi:10.1007/s11242-014-0363-y

Gili, J. A., & Alonso, E. E. (2002). Microstructural deformation mechanisms of unsaturated granular soils. *International Journal for Numerical and Analytical Methods in Geomechanics, 26*, 433–468.

Gras, J.-P., Delenne, J. Y., & El Youssoufi, M. S. (2013). Study of capillary interaction between two grains: a new experimental device with suction control. *Granular Matter, 15*, 49–56. doi:10.1007/s10035-012-0388-2

Haines, W. B. (1925). Studies of the physical properties of soils. ii. a note on the cohesion developed by capillarity forces in an ideal soil. *Journal of Agricultural Science, 15*, 529–535.

Lian, G., Thornton, C., & Adams, M. J. (1993). A theoretical study of the liquid bridge forces between two rigid spherical bodies. *Journal of Colloid and Interface Science, 161*, 138–147.

Mason, G., & Clark, W. C. (1965). Liquid bridges between spheres. *Chemical Engineering Science, 20*, 859–866.
Megias-Alguacil, D., & Gauckler, L. J. (2009). Capillary forces between two solid spheres linked by a concave liquid bridge: Regions of existence and forces mapping. *AiChE Journal, 55*, 1103–1109.
Mielniczuk, B., Hueckel, T., & El Youssoufi, M. S. (2013). Micro-scale testing of capillary bridge evolution due to evaporation. In L. Laloui & A. Ferrari (Eds.), *Multiphysical Testing of Soils and Shales*, Springer Series in Geomechanics and Geoengineering (pp. 233–238). Berlin Heidelberg: Springer.
Mielniczuk, B., Hueckel, T., & El Youssoufi, M. S. (2014). Evaporation-induced evolution of the capillary force between two grains. *Granular Matter, 16*, 815–828.
Mielniczuk, B., Hueckel, T., & El Youssoufi, M. S. (2015). Laplace pressure evolution and four instabilities in evaporating two-grain liquid bridges. *Powder Technology, 283*, 131–151. doi:10.1016/j.powtec.2015.05.024
Peron, H., Delenne, J. Y., Laloui, L., & El Youssoufi, M. S. (2009). Discrete element modelling of drying shrinkage and cracking of soils. *Computers and Geotechnics, 36*, 61–69.
Plateau, J. (1864). *The figures of equilibrium of a liquid mass* (pp. 338–369). Washington DC: The Annual Report of the Smithsonian Institution.
Princen, H. M. (1968). Comments on the effect of capillary liquid on the force of adhesion between spherical solid particles. *Journal of Colloid and Interface Science, 26*, 249–253.
Rabinovich, Y. I., Esayanur, M. S., & Moudgil, B. M. (2005). Capillary forces between two spheres with a fixed volume liquid bridge: theory and experiment. *Langmuir, 21*, 10992–10997.
Soulie, F., Cherblanc, F., El Youssoufi, M. S., & Saix, C. (2006). Influence of liquid bridges on the mechanical behaviour of polydisperse granular materials. *International Journal for Numerical and Analytical Methods in Geomechanics, 30*, 213–228.
Taubin, G. (1991). Estimation of planar curves, surfaces, and nonplanar space curves defined by implicit equations with applications to edge and range image segmentation. *IEEE Transactions on Pattern Analysis and Machine Intelligence, 13*, 1115–1138.
Willett, C. D., Adams, M. J., Johnson, S. A., & Seville, J. P. K. (2000). Capillary bridges between two spherical bodies. *Langmuir, 16*, 9396–9405.
Young, T. (1805). An essay on the cohesion of fluids. *Philosophical Transactions, 95*, 65–87. doi:10.1098/rstl.1805.0005